Stream-Specific Feedback Inputs to the Primate Primary Visual Cortex

Frederick Federer[1,†], Seminare Ta'afua[1,2,†], Sam Merlin[1,3] and Alessandra Angelucci[1]

[†] ***Equal first author contribution***

[1]Dept. of Ophthalmology and Visual Science
Moran Eye Institute
and
[2] Dept of Biomedical Engineering
University of Utah, Salt Lake City, UT 84132, USA

[3] Present address: Medical Science, School of Science, Western Sydney University, Campbelltown, NSW 2560 Australia

[*] Corresponding author and Lead Contact.

Corresponding author's address:
65 Mario Capecchi Drive
Salt Lake City, UT 84132, USA
Tel: (801) 5857489
Email: alessandra.angelucci@hsc.utah.edu

SUMMARY

The sensory neocortex consists of hierarchically-organized areas reciprocally connected via feedforward and feedback circuits. Feedforward connections shape the receptive field properties of neurons in higher areas within parallel streams specialized in processing specific stimulus attributes. Feedback connections, instead, have been implicated in top-down modulations, such as attention, prediction and sensory context. However, their computational role remains unknown, partly because we lack knowledge about rules of feedback connectivity to constrain models of feedback function. For example, it is unknown whether feedback connections maintain stream-specific segregation, or integrate information across parallel streams. Using selective viral-mediated labeling of feedback connections arising from specific cytochrome-oxidase stripes of macaque visual area V2, we find that feedback to the primary visual cortex (V1) is organized into parallel streams resembling the reciprocal feedforward pathways. These results suggest that specialized V2 feedback channels serve to modulate V1 responses to specific stimulus attributes, an organizational principle that could extend to other feedback pathways in sensory systems.

KEYWORDS: V1, V2, macaque, corticocortical, cytochrome oxidase, CO stripes, CO blobs, cortical layers, parallel processing

INTRODUCTION

In the primate sensory neocortex, information travels along multiple parallel feedforward (FF) pathways through a hierarchy of areas (Van Essen and Maunsell, 1983). Neuronal receptive fields (RFs) in higher-order areas become tuned to increasingly complex stimulus features, with multiple parallel pathways specialized in processing specific attributes of sensory stimuli (e.g. object form versus object motion). The role of FF connections in shaping cortical RFs has long been recognized (Hubel and Wiesel, 1962). In contrast, little is known about the function of feedback (FB) connections, although they have been implicated in top-down modulations of neuronal responses, such as attention (Luck et al., 1997; McAdams and Reid, 2005), prediction (Friston, 2005; Rao and Ballard, 1999) and sensory context (Angelucci et al., 2017; Hupé et al., 1998; Nassi et al., 2013; Nurminen et al., 2018). One limitation to understanding the computational function of FB is that we lack information on the rules of FB connectivity to constrain models of FB function. For example, it is debated whether FB connections are anatomically diffuse and, therefore, unspecific with respect to the functional domains they contact in lower-order areas, or whether they are patterned and functionally specific (discussed in: Angelucci and Bressloff, 2006). A related question is whether diffuse and unspecific FB connections integrate information across parallel processing streams, or whether these connections maintain stream specificity, like their reciprocal FF pathways. Answering these questions would further our understanding of FB function and allow us to refine and inspire theories of cortical computation, many of which make specific assumptions about the functional specificity, or lack thereof, of FB connections (Bastos et al., 2012; Hawkins, 2004; Mumford, 1992; Roelfsema, 2006; Shipp, 2016).

Here we have investigated the anatomical and functional organization of FB connections to the primary visual cortex (V1) arising from the secondary visual area (V2) in the macaque monkey. This FB pathway is well suited to address questions of anatomical and functional specificity and parallel FB pathways, because V2 is partitioned into cytochrome-oxidase (CO) stripe compartments that receive segregated FF projections from specific V1 CO compartments and layers (Livingstone and Hubel, 1984,1987), and CO compartments in V1 and V2 have specialized functional properties and maps (Roe et al., 2008; Sincich and Horton, 2005). It is now well established that CO blobs project predominantly to V2 CO thin stripes, while V1 interblobs project to V2 thick and pale stripes (Federer et al., 2009; Sincich and Horton, 2002). These projections arise predominantly from V1 layers (L) 2/3, and 4B, and sparsely from 4A and 5/6, with L4B projecting more heavily to thick stripes compared to other stripe types (Federer et al., 2013; Sincich et al., 2010). However, it is debated whether V2-to-V1 FB connections form similar parallel pathways that segregate within V1 CO compartments (Angelucci et al., 2002a,b; Shmuel et al., 2005), therefore maintaining stream specificity, or diffusely project to all compartments (Stettler et al., 2002), thus integrating information across parallel streams. This controversy is primarily due to the lack, in previous anatomical studies, of sensitive anterograde neuroanatomical tracers capable of labeling V2-to-V1 axons fully and selectively, without also labeling the reciprocal V1-to-V2 FF projections. Here, using selective viral-mediated labeling of FB connections arising from specific V2 CO stripes, we show that, like V1-to-V2 FF connections, V2 FB connections to V1 are organized into multiple parallel streams that segregate within the CO compartments of V1 and V2. These results suggest functionally specialized FB channels.

RESULTS

To selectively label FB connections to V1 arising from specific V2 CO stripes, we first identified the V2 stripes *in vivo*, using intrinsic signal optical imaging. We then targeted to a particular V2 stripe type injections of a mixture of Cre-expressing and Cre-dependent adeno-associated virus, serotype 9 (AAV9), carrying the gene for green fluorescent protein (GFP) or tdTomato (tdT) (see Star Methods). We have previously shown that in the primate visual cortex, this viral vector combination results in selective anterograde infection of neurons at the injected V2 site and virtually no retrograde infection of neurons in V1 (Nurminen et al., 2018). Finally, we quantified the resulting distribution of labeled FB axons across V1 layers and CO compartments. We present results from a total of 13 viral injections made in area V2 of 5 macaque monkeys. First, we describe the distribution of V2 FB axon terminals across V1 layers, and subsequently their distribution relative to CO blobs and interblobs.

Laminar Distribution of V2 Feedback Projections to V1

Figure 1 about here

Here we present results from 4 injections of the anterograde viral mixture that were made blindly into V2. Alignment of the injection sites to V2 sections stained for CO (see Star Methods) revealed that two AAV9-tdT injections were confined to thin stripes (one example is shown in **Fig. 1A-B**) and two AAV9-GFP injections encompassed all 3 stripe types, but were mostly

confined to pale-lateral stripes (one example is shown in **Fig. 1A,C**). Following Federer et al. (2013), here we term pale stripes located lateral or medial to an adjacent thick stripe as pale-lateral or pale-medial, respectively. Analysis of the laminar distribution of labeled FB axons resulting from these injections was performed on V1 tissue sectioned perpendicular to the layers along an axis parallel to the V1/V2 border. Fluorescent label was first imaged in sample sections, the same sections were then stained for CO, to reveal layers, and finally the sections were re-imaged simultaneously for both CO and fluorescent signals, to maintain perfect alignment of the FB label and CO-defined cortical layers (see Star Methods). Qualitative observations of sections imaged for GFP and tdT fluorescence (**Fig. 1D** and left panels of **Fig. 1E-F**), and quantitative analysis of fluorescent signal intensity across layers (right panels in **Fig. 1E-F**; see Star Methods for analysis details) demonstrated that V2 FB neurons terminate most densely in L1 and the upper part of L2, and in L5/6 (particularly 5B and 6). There were also weaker FB projections to the lower part of L2 and upper part of L3. A sparser projection to L4B, instead, was seen only after injections that encompassed thick and pale stripes, but not after injections confined to thin stripes. Little or no projections were seen in L4A and 4C. In the layers devoid of terminal FB axons, nevertheless, the axon trunks of labeled FB axons could be seen ascending vertically to the upper layers, but these axons did not send lateral branches in these layers.

Layer-by-layer statistical comparisons across stripe types (thin vs. all stripes) revealed a significant difference in the projections to L4B, which were virtually absent after thin stripe injections, but present when the injection encompassed also the pale/thick stripes. Moreover, injections in thin stripes resulted in significantly less projections to L6, compared to injections that additionally encompassed thick/pale stripes ($p < 0.001$ for both L4B and L6 comparisons, Mann-Whitney U test). Within each stripe group, we also statistically compared the resulting FB

label intensity across the sublayers of L4 (4A, 4B, 4C). We found no significant difference in the amount of FB projections from thin stripes to the different L4 sublayers (**Fig. 1E**). In contrast, following injections that additionally involved pale/thick stripes, L4B showed significantly denser FB terminations compared to L4A and 4C ($p < 0.001$ and $p < 0.003$, respectively, Kruskal-Wallis test with Bonferroni correction), while L4A did not differ significantly from L4C. In summary, L4B receives significant FB projections from V2 thick/pale stripes but not from V2 thin stripes, and the latter project less heavily to L6 compared to thick/pale stripes.

Figure 2 about here

Segregated Feedback Pathways from V2 Stripes to V1 Blobs and Interblobs

We next asked how FB projections from different V2 stripe types are distributed across the tangential plsane of V1. **Fig. 2A-C** shows one example case in which, using intrinsic signal optical imaging to reveal functional V2 stripes *in vivo* (see Star Methods, *Optical Imaging*), an injection of AAV9-GFP was targeted to a thin V2 stripe, and an injection of AAV9-tdT to the adjacent pale-medial stripe. In the orientation difference map, thin stripes can be identified as regions devoid of orientation responses, and pale stripes as regions with strong orientation responses neighboring a region with no orientation domains. Stripe location was confirmed postmortem on CO-stained V2 sections (**Fig. 2C**). GFP- and tdT-labeled FB projections arising from each of these two injection sites formed terminal patches in the superficial layers of V1 (**Fig. 2D-E)**. When the GFP and tdT images were merged, it was clear that, in the regions where both FB fields overlapped, GFP- and tdT-labeled patches were interleaved (**Fig. 2F**). Importantly, only axon fibers and boutons, but not somata, were labeled in the FB projection

zones, indicating these patches were formed by axonal terminations of anterogradely-labeled FB neurons (**Fig. 2G**), but not retrogradely-labeled V1 cells. These results indicated that V2 FB projections arising from distinct stripe types segregate within V1.

We next asked how the terminal patches formed by FB projections arising from each of the stripe types relate to the CO blobs and interblobs of V1, and whether patchy terminations occur throughout the V1 layers of FB termination. Below we present results from a total of 9 viral injections that were confined to V2 thick (n=3), thin (n=3) or pale (n=3) stripes.

V2 Thick Stripes Project to V1 Interblobs

Figures 3 and 4 about here

Here we present results from a total of 3 viral injections (2 AAV9-GFP, 1 AAV9-tdT, n=3 animals) that were confined to V2 thick stripes. Analysis of the distribution of labeled FB axons relative to the CO compartments of V1 was performed on tissue sectioned parallel to the pial surface. Fluorescent label was imaged in sample sections through the layers were FB axons terminated, namely L1A, 1B, 2/3, 4B and 5/6; the same or adjacent sections were then stained for CO to reveal layers and CO blobs, and imaged. Images of each section were vertically aligned in a sequential stack through the depth of V1, by aligning the radial blood vessels. One example AAV9-GFP injection site confined to a thick stripe is shown in **Figure 3**, and the FB axons in V1 labeled from this injection are shown in **Figure 4.** The left panel of **Fig. 4A** shows a filtered CO-stained section through V1 L2/3 overlapping the FB termination zone. The CO blob outlines extracted from this image (see Star Methods) are shown superimposed to the GFP-labeled axons

through the depth of V1 (left panels in **Fig. 4B-F**). Qualitative observation of these images revealed patchy FB terminations in V1, with the densest patches located preferentially in the interblobs, across all layers of FB termination. Consistent with the laminar analysis shown above, the densest terminations were located in L1/upper 2 and 5B-6, and sparser projections in L2/3 and 4B. To quantify the distribution of FB projections in the blobs and interblobs of V1, for each layer we measured fluorescent signal intensity within a square region of interest (ROI) centered on each blob overlaying the FB termination zone, and encompassing the average blob and interblob diameter in the CO map (see Star Methods and **Fig. S1**). Fluorescent signal intensity was, then, summed across all blob ROIs within a layer, and normalized to the maximum intensity value, to generate a heat map of fluorescent signals for that layer (**Figs. S1C-D, 4B-F** middle panels). The black circle on each layer heat map shows the average blob diameter estimated from the blobs used to compute that layer heat map. In all layers, the highest fluorescence intensity lay outside the average blob border, indicating the densest FB termination lay in the interblobs. The densest FB label, in this case, was located in the upper right quadrant of the heat maps, rather than uniformly filling the entire interblob region all around the blob. Indeed the densest FB label was consistently located to one side of the blobs, in the termination zone, perhaps due to the small injection site being confined to few orientation domains in the functional map of V2 (**Fig. 3B**). The heat map for L4B showed much lower fluorescent label intensity compared to the other layers, but branching axons were clearly present in this layer (**Fig. 4E**, left panel), and the highest label intensity was still found within the interblobs (**Fig. 4E,** right panel).

From each layer heat maps, we generated graphs of the normalized fluorescence signal intensity as function of distance from the center of the average blob (blue curves in right panels

of **Fig. 4B-F**), as described in the Star Methods and **Fig. S1**. These curves were compared to similarly computed curves of CO signal intensity as function of distance from the center of the average blob (black curves in right panels of **Fig. 4A-F**, which were computed from the CO heat map shown in the middle panel of **Fig. 4A**). In all layers, the CO and fluorescent signal curves showed similar trends, peaking at the largest distance from the blob center, indicating that the highest fluorescent signals coincided with the brightest regions in CO staining, i.e. the interblobs.

The other two thick stripe injection cases showed similar results to the case shown in **Fig. 4**, albeit due to the smaller size of these injections, the resulting V1 FB label was overall less dense and showed even greater specificity for the interblobs. **Figure 7A** summarizes the thick stripe population data for all layers analyzed.

V2 Thin Stripes Project to V1 Blobs

Figure 5 about here

Three viral injections (2 AAV9-GFP, 1 AAV9-tdT, n=3 animals) were confined to V2 thin stripes. One example AAV9-GFP injection site and resulting FB label in V1 are shown in **Figure 2A-D, F-G**). A second example AAV9-GFP injection site largely confined to a thin stripe (but encroaching slightly into the adjacent pale-lateral stripe) is shown in **Figure 3**, and the FB axons in V1 labeled from this injection site are shown in **Figure 5**. Analysis of the distribution of FB labeled axons was performed as for the thick stripe injection case described above. Qualitative observation demonstrated patchy FB terminations, densest in V1 L1/upper 2 and 5B-6, and sparser in L2/3, with little or no projections to L4B (**Fig. 5B-F**, left panels). Both qualitative and

quantitative analyses revealed that the densest patches of labeled FB axons lay preferentially inside the blobs, although some sparser label also occurred in the interblobs, likely due to the injection site encroaching into the adjacent pale stripe (**Fig. 5B-F**, middle and right panels). The heat map for L4B showed no significant label (**Fig. 5E**, middle panel), with noisy background label in this layer being equally distributed across blobs and interblobs (**Fig. 5E**, right panel). Qualitative observations of L4B revealed only punctate GFP label with little or no lateral axon branching, suggesting this layer mainly contained unbranched axon trunks traveling vertically (i.e. orthogonal to the plane of imaging) towards the superficial layers. This was in contrast to the branched axonal label seen in this layer after both thick (**Fig. 4E**, left panel) and pale (**Fig. 6E**, left panel) stripe injections.

The other two thin stripe injection cases showed similar results to the case shown in **Fig. 5**, but since these injection sites were more clearly confined to thin stripes, the terminal FB label showed even greater specificity for blobs. **Figure 7B** shows the thin stripe population data for all layers analyzed.

V2 Pale Stripes Project to V1 Interblobs

Figure 6 about here

Three viral injections were confined to V2 pale stripes (1 AAV9-tdT in a pale-medial stripe and two AAV9-GFP in a pale-lateral stripe, n=2 animals). One example AAV9-tdT injection site confined to a pale-medial stripe is shown in **Figure 2A-C**, and the FB axons in V1 labeled from this injection site are shown in **Figures 2E-G and 6**. FB axons from this case also showed

patchy FB terminations, densest in V1 L1/upper 2 and 5B-6, and sparser in L2/3 and L4B (**Fig. 6B-F**, left panels). FB terminals in L4B formed clear lateral branches indicative of terminations within the layer. Both qualitative and quantitative analyses revealed that the densest patches of labeled FB axons in all layers lay preferentially in the interblobs (**Fig. 6B-F**, middle and right panels). Other pale-stripe injection cases showed similar results. **Figure 7C** summarizes the pale stripe population data for all layers analyzed.

Population Analysis

Figure 7 about here

Figure 7 shows the summary data (see Star Methods) for the population of injections, grouped by stripe type (n=3 injections per stripe type). Like the individual example cases, the population data shows that FB projections arising from V2 thick and pale stripes terminate preferentially in the interblob regions of V1, across all layers of FB termination (**Fig. 7 A and C,** respectively). In contrast, FB projections arising from V2 thin stripes terminate preferentially in the CO blobs (**Fig. 7B**). Moreover, thick and pale, but not thin, stripes send FB projections to L4B. Statistical comparison of the CO compartment location of densest FB label across stripe groups, for each V1 layer, indicated no significant difference between pale and thick stripes (L1A: $p=0.33$; L1B: $p=0.38$; L2/3: $p=0.99$; L4B: $p=0.56$; L5/6: $p=0.98$; Kruskal-Wallis test with Bonferroni correction). In contrast, the CO compartment location of FB projections to V1 differed significantly between thick and thin stripes, as well as between thin and pale stripes, and this was the case for all layers of FB termination ($p < 0.001$ for all comparisons and all layers but L4B),

except for L4B for which there was no significant difference between thick and thin stripes ($p = 0.01$), or thin and pale stripes ($p= 0.053$). Moreover, when all layers data were pooled together for each stripe group (see Star Methods), V2 thick and pale stripes showed no significant difference in the V1 CO compartment location of their projections ($p = 0.801$), while thick versus thin, and thin versus pale stripes were significantly different from each other ($p < 0.001$ for all comparisons).

DISCUSSION

Figure 8 about here

We have shown that FB projections arising from the different CO stripes of V2 do not diffusely and unspecifically contact all V1 regions within their termination zones, but rather form patchy axon terminations which largely segregate in the CO compartments of V1: thin stripes project predominantly to blobs and thick and pale stripes predominantly to interblobs. Moreover, all stripes types send densest projections to layers 1/upper 2 and 5B-6, and sparser projections to lower layer 2 and layer 3. However, only thick and pale, but not thin, stripes project to L4B (**Fig. 8**).

There has been a long-standing controversy regarding the clustering and specificity, or lack thereof, of FB connections to V1, mainly attributable to the technical limitations of the neuroanatomical tracers used in previous studies (discussed in: Angelucci and Bressloff, 2006). Conventional tracers used to label FB axons were either transported anterogradely, but had poor sensitivity and resolution (e.g. tritiated aminoacids, WGA-HRP, and first generation adenoviral vectors), or had good sensitivity, but were transported bidirectionally (CTB, BDA), thus labeling

the axons of both FF- and FB-projecting neurons. Studies using the first group of tracers injected in areas V2 or MT concluded that FB connections to V1 are diffuse, i.e. they make non-clustered terminations in their target areas, which are non-specific with respect to the CO compartments or functional domains of V1 (Maunsell and Van Essen, 1983; Rockland and Pandya, 1979; Stettler et al., 2002). Studies using injections of bidirectional tracers into V2, instead, provided evidence for clustered and functionally-specific V2 FB projections to V1 (Angelucci et al., 2002b; Shmuel et al., 2005). Due to the bidirectional transport of the tracers used in the latter studies, however, it was unclear whether the axon clustering reflected the termination patterns of FB axons or of the axonal collaterals of the reciprocal FF projection neurons, known to form patchy connections (Federer et al., 2009; Livingstone and Hubel, 1988; Sincich and Horton, 2002). For the same reason, it had remained unclear whether FB projections to V1 terminate only in L1 and 6 (which do not send, or only send very sparse, FF projections to extrastriate areas), or also terminate in layers that send FF projections to higher cortical areas (such as L2/3 and 4B). In a few studies, FB axons were labeled by bulk injections of PHA-L or BDA in V2 or MT, and reconstructed through serial sections (Anderson and Martin, 2009; Rockland and Knutson, 2000; Rockland and Virga, 1989). While these studies were not affected by ambiguity in the interpretation of the origin of axonal label, they, however, provided a limited sample of partially reconstructed FB axons.

To overcome the limitations of previous anatomical studies, in this study we have taken advantage of recent advances in neuroanatomical labeling methods based on the use of viral vectors to deliver genes for fluorescent proteins (Luo et al., 2008). Specifically, we have used a mixture of AAV9-Cre and Cre-dependent-AAV9 to express fluorescent proteins in V2 FB neurons projecting to V1 without simultaneously labeling the axons of the reciprocal V1-to-V2

FF projection neurons. Our results resolve existing controversies by demonstrating unequivocally that FB connections from V2 to V1 form patchy terminations that are predominantly CO-compartment specific. In particular, we demonstrate that in macaque monkey, FB connections arising from the different CO stripes of V2 form parallel channels that mimic the reciprocal parallel pathways from V1 to V2 in this species (Sincich and Horton, 2002). We also show that, with the exception of L1, the layers that give rise to FF connections to V2 (2/3, 4A, 4B, 5/6) receive reciprocal FB inputs. This suggests that V2 FB axons may make direct contacts with V1 neurons sending FF inputs to V2, an hypothesis that we are currently testing (Siu et al., 2018). However, while L4B has been shown to send at least some sparser inputs to thin and pale-medial stripes (Federer et al., 2013; Sincich et al., 2007, 2010), we only observed significant FB inputs to L4B from thick and pale, but not thin, stripes. It is possible that our method of analysis failed to capture very sparsely labeled FB axons in L4B arising from thin stripes. Moreover, our low sample of injections into pale-medial stripes (n=1) did not allow us to assess potential quantitative differences in the FB projections to L4B from the two pale stripe types, as has been previously demonstrated for the L4B-to pale stripe FF projections (Federer et al., 2013). In this study we have not analyzed L4A for potential FB terminations, as this very thin layer is difficult to study in tangential sections, and in pia-to-white matter sections FB projections to L4A appeared to be, at best, very sparse.

Although here we are proposing the existence of at least 3 segregated FB pathways from V2 to V1, our study shows that FB projections from thick and pale stripes both terminate in the interblobs, allowing for the possibility that these projections contact the same V1 cells, therefore integrating information across these two parallel streams. Current studies from our laboratory, using rabies virus-mediated monosynaptic input tracing to label direct inputs to V2-projecting

neurons in V1, however, indicate that FB projections from thick and pale stripes contact predominantly distinct V1 projection neurons (Siu et al., 2018).

Segregation of V1-to-V2 FF pathways within CO compartments likely reflects specialized function, because CO compartments in V1 and V2 show specialized neuronal responses properties and functional maps. Specifically, the blob-thin-stripe pathway is thought to process surface properties (color and brightness), the interblob-pale stripe pathway object contours and form, and the interblob-thick stripe pathway object motion and depth (Chen et al., 2008; DeYoe and Van Essen, 1985; Landisman and Ts'o, 2002; Livingstone and Hubel, 1988; Lu et al., 2010; Lu and Roe, 2008; Tootell et al., 1988, 2004; Ts'o and Gilbert, 1988; Wang et al., 2007; Xiao et al., 2003, 2007; Yoshioka and Dow, 1996). Our finding of segregated FB projections within these same CO compartments, therefore, suggests that V2 FB connections to V1 do not integrate information across parallel functional streams, and thus across stimulus attributes, but rather modulate V1 responses to the specific stimulus attributes that are processed within their functional stream, an organization that may support, for example, feature-selective attention (Maunsell and Treue, 2006; Moore and Zirnsak, 2017), or the feature specificity of extraclassical receptive field effects (Albright and Stoner, 2002; Angelucci et al., 2017; Angelucci and Shushruth, 2013).

Our finding of segregated V2-toV1 FB pathways is consistent with previous results of stream specific organization of corticogeniculate pathways in macaque (Briggs et al., 2016; Briggs and Usrey, 2009), suggesting this FB organization may exist at multiple levels of the visual pathway. Our results are also consistent with results in mouse visual cortex, demonstrating segregation of functional FB channels from L5 of higher visual areas AL (anterolateral) and PM

(posteromedial) to V1 (Huh et al., 2018), which also matches the functional segregation of the reciprocal FF pathways from V1 to AL and PM (Glickfeld et al., 2013).

Our results of segregated FB pathways are consistent with predictive coding theories of FB function. According to these theories, the brain generates an internal model of the world, based on sensory data and prior experience, which is refined by incoming sensory data. The latter is compared to the predicted sensory data, and it is the prediction error that ascends up the cortical hierarchy and refines the higher levels' model (Friston, 2008; Friston and Kiebel, 2009; Rao and Ballard, 1999). Predictive coding models postulate the existence of different neuronal populations encoding expectations and prediction errors, respectively, at each level of the cortical hierarchy. In these models, inter-areal FB connections carry the predictions, while FF connections carry the error in those predictions (Bastos et al., 2012; Shipp, 2016). In terms of the architecture of hierarchical predictive coding schemes, one key attribute is the functional segregation of conditionally independent expectations, so that descending predictions are limited to prediction errors reporting a particular stimulus attribute, but not prediction errors reporting opposite or different attributes. For example, predictions about the orientation of a visual edge should not project to prediction errors units encoding visual motion (because knowing the orientation of an edge does not, statistically, tell us anything about its motion). This suggests that direct descending predictions will be largely specific for stimulus attributes (e.g., contours vs. motion), which is consistent with our finding of FB-specific channels.

Acknowledgments

We thank Kesi Sainsbury for technical assistance, and Dr. Jeff Yarch for help with some experiments. Supported by grants from NIH (R01 EY026812, R01 EY019743, BRAIN U01

NS099702), NSF (IOS 1755431, EAGER 1649923), University of Utah Research Foundation and Neuroscience Initiative, to A.A., and from Research to Prevent Blindness, Inc. and a core grant from NIH (EY014800) to the Department of Ophthalmology, University of Utah.

Author Contributions

Conceptualization: all authors. Methodology: all authors. Software: S.T. Validation: S.T., F.F., A.A. Formal Analysis: S.T. Investigation: F.F., S.M., A.A. Writing-Original Draft: F.F., S.T., A.A. Writing–Review/Editing: all authors. Visualization: F.F., S.T. Supervision & Funding Acquisition: A.A.

Declaration of Interests

The authors declare no competing interests.

FIGURE LEGENDS

Figure 1. Laminar Distribution of V2 Feedback Projections to V1.

Case MK359LH. **(A)** Micrograph of a merged stack of V2 sections stained for CO, to reveal the stripes (delineated by *dashed white contours*). *Red and green ovals* are the composite outlines of an AAV9-tdT and AAV9-GFP injection site, respectively, taken from (B-C) and overlaid onto the V2 CO stack. *TN:* thin stripes. **(B-C)** Micrographs of an AAV9-tdT and an AAV9-GFP injection site, respectively, taken under fluorescent illumination. While the images are from a single tissue section, the *red and green outlines* mark the full extent of the injection sites through the layers, and were generated by aligning images of injection sites through the depth of the cortex. **(D)** Image of CO-stained section through the layers of V1 (indicated on the right side). *White dashed* contours delineate layer boundaries, and the CO blobs in L2/3. The same tissue section, but imaged for fluorescent label, is illustrated in (E) and (F). **(E)** <u>LEFT:</u> Image of tdT-labeled FB axons through V1 layers resulted from the thin stripe injection shown in panels (A-B). <u>RIGHT</u>: Population average of normalized fluorescent signal intensity across V1 layers following thin stripe injections (n=2). **(F)** Same as (E) but for FB label resulted from injections (n=2) that were centered on a pale-lateral stripe, but spilled into adjacent thick and thin stripes. Scale bar under left panel in (F) is valid for (D) and left panel in (E).

Figure 2 Segregated V2-toV1 Feedback Pathways.

Case MK374RHLat. **(A)** Difference orientation map of V1 and V2 obtained by subtracting responses to achromatic luminance gratings of 135° orientation from gratings of 45° orientation, recorded using *in vivo* intrinsic signal optical imaging. *Horizontal dashed white contour*: V1/V2

border. *Dashed cyan contours* delineate regions devoid of orientation responses, corresponding to thin stripes (*TN*); *dashed white contours* are outlines of the thin stripes in CO staining (C), which were superimposed onto the optical map in (A) by aligning the superficial blood vessels in the top histological section with *in vivo* images of the cortical surface vasculature (see Star Methods). Note good correspondence of CO-defined and functionally-defined thin stripes. *The black box here and in (C)* frame the same V1 region in the optical map and CO stained sections. *Green and red ovals* are the composite outlines of an AAV9-GFP and an AAV9-tdT injection site, respectively, from (B). **(B)** Micrographs of the AAV9-GFP and AAV9-tdT injection sites, respectively, taken under fluorescent illumination. The green and red ovals outline the composite injection site through the layers and are shown overlaid onto the V2 optical map in (A) and the V2 CO sections in (C). **(C)** CO-stained tissue section through V2, revealing the stripe pattern and the location of the two injection sites (ovals). **(D)** Micrograph of a V1 section through L1B of V1 seen under GFP fluorescence, showing patchy terminations of GFP-labeled FB axons. *Arrowheads* point to same blood vessels in (D-F). **(E)** Same section as in (D), but seen under tdT fluorescence, showing patchy terminations of tdT-labeled FB axons. **(F)** Merge of images in (D) and (E). Label inside the *white box* is shown at higher power in (G). **(G)** High power view of FB terminations demonstrating lack of labeled somata, indicating the viral vectors acted as selective anterograde tracers.

Figure 3. Injection sites in V2 thick and thin stripes.

Example of two AAV9-GFP injection sites, one confined to a V2 thick stripe, the other to a thin stripe, in case MK356RH. **(A)** Difference color map in V2 obtained by subtracting averaged optical responses to red-green and blue-yellow pairs of full field square stimuli from responses to

achromatic black-white square pairs. *Dashed yellow contours* delineate regions of strong color responses, corresponding to thin stripes; *white dashed contours* here and in (B) are the outlines of the thin stripes in CO staining (C), which were overlaid to the optical maps (as for **Fig. 2A**). **(B)** Difference orientation map of the same V2 region as in (A) obtained by subtracting optical responses to achromatic luminance gratings of 135° orientation from gratings of 45° orientation. *Dashed cyan contours* delineate regions devoid of orientation responses, corresponding to thin stripes. There is good correspondence between functionally-defined and CO-defined thin stripes. *Green ovals* here and in panels (C-D) are the composite outlines of the two AAV9-GFP injection sites shown in (D). **(C)** Stack of aligned and merged V2 tissue sections stained for CO, revealing the stripe pattern, in the same V2 region as in (A-B). **(D)** Micrographs of the two AAV9-GFP injection sites taken under fluorescent illumination.

Figure 4. V2 Thick Stripes Project to V1 Interblobs.

Case MK356RH. GFP-labeled FB axons in V1 after the thick stripe injection shown in **Figure 3**. **(A)** <u>LEFT:</u> filtered CO map from a tissue section through V1 L2. Segmenting out the darkest 33% of pixels outlines the CO blobs (*yellow outlines*). Scale bar valid also for left panels in (B-F). <u>MIDDLE:</u> heat map of CO signal intensity, generated by measuring CO intensity within a 476μm^2 ROI centered around each blob used for the analysis of this case, summing all case ROIs and normalizing to maximum intensity (see Star Methods and **Fig. S1D**). The average blob diameter (*black circle*) for this case was 284μm. <u>RIGHT:</u> plot of the normalized CO signal intensity as a function of distance from the blob center (B_{ctr}), computed from the CO heat map, as described in the Star Methods and **Fig. S1D-E**. CO intensity is darkest in the B_{ctr} and brightest in the center of the interblob (I_{ctr}). The black CO-intensity curve is repeated on each plot in the

right panels of (B-F) for comparison with the FB-label intensity curves. **(B-F)** LEFT: GFP-labeled FB axons in different V1 layers (cortical layer is indicated at the bottom left corner of each panel) with superimposed the blob outlines (*yellow)* from (A, left). *Dashed white lines in (B)* outline the pial vessels. MIDDLE: heat maps of the GFP-label intensity for each respective layer, generated by measuring fluorescent signal intensity within an ROI centered on each blob overlaying the FB label in that layer, summing all ROIs, and normalizing to maximum intensity. The size of the ROI in each layer reflected the average blob and interblob size within the FB termination zone in that layer (see Star Methods and **Fig. S1A-C**). *Black circles*: average blob diameter for the blobs used to compute the heat map for that layer. RIGHT: plots of normalized CO (*black curves*) and GFP-fluorescence (*blue curves*) intensities as a function of distance from the B_{ctr}, computed as described in the Star Methods and **Fig. S1C-E**. Same conventions are used in **Figures 5-7**.

Figure 5. V2 Thin Stripes Project to V1 Blobs

Case MK356RH. Same as in **Figure 4**, but for GFP-labeled FB axons in V1 resulting from the AAV9-GFP injection site confined to a V2 thin stripe shown in **Figure 3**.

Figure 6. V2 Pale Stripes Project to V1 Interblobs

Case MK374RHLat. Same as in **Figure 4**, but for tdT-labeled FB axons in V1 resulting from the AAV9-tdT injection site confined to a pale-medial stripe shown in **Figure 2A-C**.

Figure 7. Population Analysis

Heat maps and plots of fluorescent signal intensity, and plots of CO signal intensity for the population of FB projections arising from **(A)** V2 thick stripes (n=3), **(B)** thin stripes (n=3), and **(C)** pale stripes (n=3). For details of how the population averages were computed see Star Methods. Error bars in the fluorescent signal intensity plots are s.e.m. Conventions are as in **Fig. 4**.

Figure 8. Parallel V2-to-V1 Feedback Pathways.

Our proposed model of the FB pathways from V2 to V1, based on the present study. The arrow thickness indicates the relative density of projections to the different V1 layers (L4A is omitted). For all stripe types, layers 1/upper 2 and 5/6 receive the densest FB projections, while lower L2 and L3 receive sparser projections from V2. Both thick (*blue arrows*) and pale (*green arrows*) stripes, but not thin (*red arrows*) stripes send FB projections to V1 L4B. FB projections from thin stripes predominantly target the V1 CO blob columns, while FB projections from thick and pale stripes predominantly target the V1 interblob columns.

STAR METHODS

Lead Contact And Materials Availability

Further information and requests should be directed to, and will be fulfilled by, the Lead Contact, Alessandra Angelucci (alessandra.angelucci@hsc.utah.edu). This study did not generate new unique reagents.

Experimental Model and Subject Details

Five adult (4 females, 1 male) cynomolgus macaque monkeys (*Macaca fascicularis)* were used in this study. All procedures involving animals were approved by the Institutional animal Care and Use Committees of the University of the Utah and conformed to the guidelines set forth by the USDA and NIH.

Method Details

AAV9 vectors carrying the gene for either GFP or tdT were injected into specific V2 stripes, which in most cases were identified *in vivo* by intrinsic signal optical imaging. In two animals, instead, injections were made blindly with respect to stripe type. The V1 laminar and CO compartment distribution of resulting labeled FB axons was analyzed quantitatively.

Surgical Procedures

Animals were pre-anesthetized with ketamine (10-20 mg/kg, i.m.), intubated with an endotracheal tube, placed in a stereotaxic apparatus, and artificially ventilated. Anesthesia was maintained with isofluorane (0.5–2.5%) in 100% oxygen, and end tidal CO_2, blood oxygenation

level, electrocardiogram, and body temperature were monitored continuously. The scalp was incised, a craniotomy was made to expose the lunate sulcus and about 5 mm of cortex posterior to it (encompassing V2 and a small portion of V1). In two animals (MK359, 4 injections, and MK365, 3 injections) small durotomies were made just caudal to the posterior edge of the lunate sulcus, over V2, and viral vectors were injected into V2. In the reminder of cases (3 animals, total of 12 injections), optical imaging was used to identify the V2 stripes prior to the injections. In the latter cases, a large craniotomy and durotomy (15-20 mm mediolaterally, 6-8mm anteroposteriorly) were performed to expose V2 and parts of V1, a clear sterile silicone artificial dura was placed on the cortex, and the craniotomy was filled with a sterile 3% agar solution and sealed with a glass coverslip glued to the skull with Glutures (Abbott Laboratories, Lake Bluff, IL). On completion of surgery, isoflurane was turned off and anesthesia was maintained with sufentanil citrate (5–10 μg/kg/h, i.v.). The pupils were dilated with a short-acting topical mydriatic agent (tropicamide), the corneas protected with gas-permeable contact lenses, the eyes refracted, and optical imaging was started. Once the V2 stripes were functionally identified (1-4 hrs of imaging, see below), the glass coverslip, agar and artificial dura were removed and the viral vectors were injected in specific V2 stripe types, using surface blood vessels as guidance. On completion of the injections, new artificial dura was placed on the cortex, the craniotomy was filled with Gelfoam and sealed with sterile parafilm and dental cement, the skin was sutured and the animal was recovered from anesthesia. Animals survived 3-4 weeks post-injections, and underwent a terminal 3-5 day optical imaging experiment to obtain additional functional maps. At the conclusions of this experiment the animal was sacrificed with Beuthanasia (0.22 ml/kg, i.v.) and perfused transcardially with saline for 2–3 min, followed by 2 or 4% paraformaldehyde in 0.1 M phosphate buffer for 15-25 min.

Injections of Viral Vectors

A total of 19 viral vector injections were made in 5 macaque monkeys. We excluded from analysis 6 injections, which either did not produce detectable label in V1 (n=2), or were located in an unidentifiable stripe (n=4). The viral vectors consisted of a 1:1 mixture of AAV9.CaMKIIa.4.Cre.SV40 and either AAV9.CAG.Flex.eGFP.WPRE.bGH or AAV9.CAG.Flex.tdTomato.WPRE.bGH (Penn Vector Core, University of Pennsylvania, PA), which were mixed and loaded in the same glass micropipette (tip diameter 35-45 µm), and pressure injected using a picospritzer. At each injection site, 100-300 nl of the viral mixture were slowly injected (6-15 nl per min) at a cortical depth of 0.8-1.2 mm from the pial surface. After a 5 min pause, the pipette was retracted to a depth of 0.5-0.6 mm, and an additional 100-300 nl of the viral mixture were injected at the same speed. The pipette was left in place for an additional 5-10 min before being retracted. In one case (MK356), we made an injection of 750 nl at a single cortical depth (1 mm) in a thick stripe, and a second injection of 1,000 nl at 1 mm depth in a thin stripe. These injection parameters yielded injection sites ranging between 500 and 1,000 µm in diameter, involving all V2 layers. Each animal received 2-5 injections in dorsal area V2 of one hemisphere. Within the same hemisphere either vectors expressing different fluorophores (GFP or tdT) were injected, or injections of the same vector were spaced at least 10 mm apart, to ensure no overlap of the resulting labeled fields in V1. In one case (MK356), instead, two injections of the GFP-expressing vector were made in a thick and a thin stripe within the same V2 stripe cycle (**Fig. 3**), which resulted in two labeled fields in V1 that slightly overlapped. In this case, we excluded from analysis the region of label overlap.

Optical Imaging

Acquisition of intrinsic signals was performed using the Imager 3001 (Optical Imaging Ltd, Israel) under red light illumination (630 nm). To identify the V2 stripes, we imaged for orientation and color responses. Orientation maps were obtained by presenting full-field, high contrast (100%), pseudorandomized, achromatic drifting square-wave gratings of eight different orientations at 1.0-2.0 cycles per degree spatial frequency, moving back and forth at 1.5 or 2 degrees per second in directions perpendicular to the grating orientation. Responses to same orientations were averaged across trials, baseline subtracted, and difference images obtained by subtracting the responses to two orthogonal oriented pairs (e.g. **Figs. 2A, 3B**). Imaging for color responses (e.g. **Fig. 3A**) was performed by presenting isoluminant chromatic gratings (red/green and blue/yellow pairs) at 4 orientations every 500ms, pseudorandomized with presentation of achromatic luminance gratings. Averaged color responses were then subtracted from the averaged response to the blank and achromatic stimuli. Thick stripes were identified as the middle of regions having an orientation-preference map (e.g. **Fig. 3B**); pale stripes as regions having an orientation-preference map neighboring a region devoid of orientation maps (e.g. **Fig. 2A**); and thin stripes as regions containing domains responsive to color, but devoid of orientation maps (e.g. **Figs. 2A, 3B**). In each case, reference images of the surface vasculature were taken under 546 nm illumination, and used *in vivo* as reference to position pipettes for viral vector injections, as well as postmortem to align the functionally identified V2 stripes to the histological sections containing the injection sites and sections labeled for CO to reveal the stripes (e.g. **Figs 2A-C, 3**).

Histology

Areas V1 and V2 were dissected away from the rest of the visual cortex. The block was postfixed for 1-2 h, sunk in 30% sucrose for cryoprotection, and frozen-sectioned at 40 µm. For the laminar analysis the block was cut perpendicularly to the layers and parallel to the V1-V2 border. For the cases in which optical imaging was performed, instead, the block was postfixed between glass slides for 1-2 h to slightly flatten the cortex in the imaged area, cryoprotected, and frozen-sectioned parallel to the plane of the imaging camera. Sections were wet-mounted and imaged for fluorescent GFP and tdT-labeled cell bodies in V2 (the injection sites) and FB axons in V1 using either Zeiss Axioskop 2 or Axio Imager Z2 microscopes (10x magnification). After digitizing the sections, in most cases, the same sections were reacted for CO to reveal the cortical laminae and V1 and V2 compartments, and then re-imaged under bright field illumination (1.25x-5x magnification). In some instances, sections were further immunoreacted to enhance the GFP signal strength, and then imaged a third time using both bright field and fluorescent channels to maintain a perfect alignment between the CO and label images. In a few instances, CO staining was obtained from adjacent sections rather than from the same section imaged for fluorescent label, and sections were aligned by registering the radial blood vessels.

Quantification and Statistical Analysis

Analysis of Injection Site Location

Digitized fluorescent label and CO-staining from the same or adjacent sections were aligned, using IRTweak and Photoshop software, by registering the radial blood vessels sequentially in a stack encompassing all cortical layers (for the tangentially sectioned cases). CO-staining was used to assign injection sites to specific V2 CO stripes. To determine the CO stripe location of

the injection sites, typically 3-6 images of serial CO sections were overlaid by aligning the radial blood vessels and merged in Adobe Photoshop. This approach reveals a more complete stripe pattern than any individual CO-stained section, in which the stripes can be incomplete. V2 injection sites were outlined through multiple images of serial injection sites, spanning the depth of the cortex; a composite injection site encompassing all outlines in individual sections was overlaid onto the merged CO stack, and its size and stripe location were determined. The size of the injections was defined as the region at the injection site where labeled cell bodies could be discerned, as the viral vectors we used infect neuronal somata. Dark CO stripes were classified as thick (or thin) if they appeared thicker (or thinner) than the two adjacent dark stripes in CO staining and coincided with thick (or thin) stripes as defined in the optical imaging maps (see above ***Optical Imaging***), for cases in which imaging was available.

Laminar Distribution of FB Axons: Quantitative Analysis

For each injection case used for the laminar analysis (n=4), the V1 laminar distribution of labeled V2 FB axons was analyzed in 3 tissue sections (cut perpendicular to the cortical layers), of which one section was selected near the center of the FB labeled field, where FB terminations are densest, and 1 section was selected on each side of this center section, equally spaced across the full extent of the labeled field in L4B (as the FB labeled field in this layer had a smaller tangential extent than the labeled fields in other layers, and we wanted the ROI chosen for analysis to include all layers of FB termination). Sections were imaged for GFP and tdT fluorescent label, stained for CO (to reveal layers), then re-imaged for both CO staining and fluorescent label. The layer boundaries were traced manually using CO staining. For each section selected for quantitative analysis, a ROI (500 μm wide, the full length of the cortex) was

centered on the area that contained the densest fluorescent label. The ROI was further binned from top of the cortex to the white matter border into 100 bins. Individual pixel fluorescent intensity values were measured within each bin, and averaged to obtain the label intensity per bin. The different bin intensities were then normalized to the maximum bin intensity in that ROI. The binning of the ROI provided a FB label intensity profile across the cortical depth. The normalized label intensity in each bin was finally averaged across the 3 section ROIs and, again, normalized to the max average intensity to produce a single V1 laminar profile of the label intensity for each injection case. Population laminar profiles for FB arising from the same V2 stripe type were obtained by averaging the laminar profiles across cases with injections in the same stripe type. The cortical layer boundaries derived from the average layer thickness across CO-stained sections were then superimposed to the label laminar profile (right panels in **Fig. 1E,F**).

To determine whether viral injections in different V2 stripe types produced different laminar profiles, we performed statistical comparisons on a layer-by-layer basis. Because layers can vary in thickness across different sections, and therefore ROIs, in this analysis the same layer could contain slightly different numbers of bins across ROIs, each having an average pixel intensity value. The *n* for a given layer dataset consisted of the average intensity value of each bin in that layer across all ROIs, pooled across all cases with an injection in the same V2 stripe type. For across stripe statistical comparison of FB label intensity for each layer, we used a nonparametric test for to independent samples (Mann-Whitney U test - using the Matlab's *ranksum* function), due to the varying number of bins per layer and the non normal distribution of the data.

For each stripe group, we also statistically compared the resulting FB label intensity across the sublayers of L4 (4A, 4B, 4C). The *n* for the sublayer dataset consisted of the average intensity value of each bin in that sublayer across all ROIs, pooled across all cases with an injection in the same V2 stripe. For statistical comparison we used the Kruskal-Wallis test with a Bonferroni corrected α value of 0.017.

CO Compartment Distribution of FB Axons: Quantitative Analysis

This analysis was performed on tissue sectioned tangentially to the pial surface. For each injection case used for this analysis (n= 9 injections, 3 for each stripe type), digitized images of fluorescent label and CO staining were warped and aligned into a sequential stack through the depth of the cortex. CO staining was used to identify layers, as well as the blobs and interblobs in the superficial layer sections. For each case, we selected for quantitative analysis at least one section (the one with the densest label) through each of the following layers: 1A, 1B, 2/3, 4B, 5/6. However, for some layers (particularly the thinner L1A, 1B and 4B), in some cases it was necessary to select for analysis two adjacent sections, because the cut was not perfectly tangential and therefore the label field in that layer was split between adjacent sections; this ensured that the entire labeled FB field for that layer was analyzed. To quantify the distribution of labeled FB axons across V1 CO compartments within each of the chosen sections, we extracted from a L2/3 CO-stained section in the aligned section stack the CO blob borders, blob centers and interblob center-lines (**Fig. S1A**). Blob borders were extracted by processing digitized images of CO stained sections using low-pass and equalization filters (using Image Pro Inc. software), and segmenting out the darkest 33% of pixels across the gray scale image (yellow outlines in **Fig. S1A**) (Boyd and Casagrande, 1999; Federer et al., 2009). Blob centers were

defined as the darkest spot within each blob (red dots in **Fig. S1A**), as determined by the image analysis software; the latter were then visually inspected for accuracy. For blobs that showed significant elongation, we marked several centers; the latter generally coincided with multiple peaks in CO intensity along the length of the blob, having similar center-to-center spacing as the surrounding tissue (e.g. see several elongated blobs in **Fig. S1A**). The centers of the interblobs were defined as the brightest pixels between adjacent blob centers (green outlines in **Fig. S1A**).

For each injection case, we analyzed the CO map in V1 L2/3 encompassing the full tangential extent of the labeled FB fields across the layers. From this CO map we estimated a square region of interest (ROI; black box in **Fig. S1A**) whose size encompassed the average blob and interblob size in the map. To estimate the ROI, for each blob in the CO map, we computed a mean blob center-to-interblob center (B_{ctr}-I_{ctr}) distance from radial distances measured at 20° increments around the blob center. A grand average B_{ctr}-I_{ctr} distance was then computed from all relevant blobs' mean B_{ctr}-I_{ctr} distances. This grand average distance was doubled to obtain the ROI for that case. This ROI was then centered on each blob in the CO map, and the CO staining intensity was measured for each pixel within each blob ROI, summed across all blob ROIs, and normalized to the maximum summed intensity value, to produce a CO intensity heatmap for the case (**Fig. S1B**). Mean blob diameter for the case was computed from all blobs used for the analysis and overlaid onto the CO heatmap (black circle in **Fig. S1B**).

In a similar fashion we generated heatmaps of fluorescent FB label (GFP or tdT) intensity for each layer of FB termination, by measuring fluorescent intensity within the same size ROI used to compute the CO heatmap, centered on each blob in the CO map that overlaid the labeled FB field in that layer (**Fig. S1C**). Therefore the number of blobs used for this analysis could vary from layer to layer, depending on the extent and location of the labeled fields in each layer.

Signal intensity was summed across all ROIs in the layer, and normalized to the maximum intensity, to produce a fluorescent intensity heatmap for that layer (**Fig. S1D)**. A mean blob diameter specific to each layer was computed from all blobs used to generate each layer heatmap, and overlaid onto the layer heatmap (black circle in **Fig. S1D**).

From the heat maps, we generated graphs of the normalized CO or fluorescence signal intensity as function of distance from the blob center (**Fig. S1E**). Because the distribution of FB label was not homogenous all around the blobs (e.g. **Fig. S1D**), these graphs were generated by measuring the average signal intensity in each of 20 bins spanning from the center of the blob (zero on the x axis) to the center of the interblob (1.0 on the x axis) within a 200 µm-wide window centered in the region of highest signal intensity in the heat map (black boxes in **Fig. S1B,D**); signal intensity was finally normalized to the maximum bin intensity value. The region of highest intensity on the heat map was determined by measuring the average signal intensity within a 200µm-wide window rotated every 20° around the blob center, and selecting the window with the highest average signal intensity. As the latter was measured independently on the CO and fluorescence heatmaps, their respective windows of highest signal intensity did not necessarily match in location around the average blob center (e.g. in **Fig. S1D**, the window is located at 90°, while in **Fig. S1D** it is located at 290°).

To produce population heatmaps for each cortical layer (**Fig. 7**), the layer heatmaps from each case were scaled up to the largest heatmap across the relevant cases, summed and normalized to the maximum summed value. The population graphs in **Fig. 7** were generated from the population heat maps as described above for the individual cases (**Fig. S1E**).

We statistically compared the location of densest FB label produced by injections in different stripe type. To this purpose, for each case layer heatmap, within the 200µm window of

densest label, out of the 20 bins we selected for analysis those with >70% intensity. The locations of the selected bins relative to the blob center were compared layer by layer across stripe types. For statistical comparison across stripes we used a Kruskal-Wallis test with a Bonferroni corrected α value of 0.017. We also performed a statistical comparison by pooling all the selected bin locations across all layers for a given stripe type and comparing across stripe types, again using Kruskal-Wallis test with Bonferroni correction.

Data and Code Availability

The Matlab code used to generate the heatmaps and perform data analyses in this study are found on GitHub at https://github.com/angeluccilab/streamspecificfeedback.

REFERENCES

Albright, T.D., and Stoner, G.R. (2002). Contextual influences on visual processing. Ann. Rev. Neurosci. *25*, 339-379.

Anderson, J.C., and Martin, K.A.C. (2009). The synaptic connections between cortical areas V1 and V2 in macaque monkey. J. Neurosci. *29*, 11283-11293.

Angelucci, A., Bijanzadeh, M., Nurminen, L., Federer, F., Merlin, S., and Bressloff, P.C. (2017). Circuits and mechanisms for surround modulation in visual cortex. Ann. Rev. Neurosci. *40*, 425-451.

Angelucci, A., and Bressloff, P.C. (2006). The contribution of feedforward, lateral and feedback connections to the classical receptive field center and extra-classical receptive field surround of primate V1 neurons. Prog. Brain Res. *154*, 93-121.

Angelucci, A., Levitt, J.B., and Lund, J.S. (2002a). Anatomical origins of the classical receptive field and modulatory surround field of single neurons in macaque visual cortical area V1. Prog. Brain Res. *136*, 373-388.

Angelucci, A., Levitt, J.B., Walton, E., Hupé, J.M., Bullier, J., and Lund, J.S. (2002b). Circuits for local and global signal integration in primary visual cortex. J. Neurosci. *22*, 8633-8646.

Angelucci, A., and Shushruth, S. (2013). Beyond the classical receptive field: surround modulation in primary visual cortex. In The new visual neurosciences, L.M. Chalupa, and J.S. Werner, eds. (MIT press), pp. 425-444.

Bastos, A.M., Usrey, W.M., Adams, R.A., Mangun, G.R., Fries, P., and Friston, K.J. (2012). Canonical microcircuits for predictive coding. Neuron *76*, 695-711.

Boyd, J.D., and Casagrande, V.A. (1999). Relationships between cytochrome oxidase (CO) blobs in primate primary visual cortex (V1) and the distribution of neurons projecting to the middle temporal area (MT). J. Comp. Neurol. *409*, 573-591.

Briggs, F., Kiley, C.W., Callaway, E.M., and Usrey, W.M. (2016). Morphological Substrates for Parallel Streams of Corticogeniculate Feedback Originating in Both V1 and V2 of the Macaque Monkey. Neuron *90*, 1-12.

Briggs, F., and Usrey, W.M. (2009). Parallel processing in the corticogeniculate pathway of the macaque monkey. Neuron *62*, 135-146.

Chen, G., Lu, H.D., and Roe, A.W. (2008). A map for horizontal disparity in monkey V2. Neuron *58*, 442-450.

DeYoe, E.A., and Van Essen, D.C. (1985). Segregation of efferent connections and receptive field properties in visual area V2 of the macaque. Nature *317*, 58-61.

Federer, F., Ichida, J.M., Jeffs, J., Schiessl, I., McLoughlin, N., and Angelucci, A. (2009). Four projections streams from primate V1 to the cytochrome oxidase stripes of V2. J. Neurosci. *29*, 15455-15471.

Federer, F., Williams, D., Ichida, J.M., Merlin, S., and Angelucci, A. (2013). Two projection streams from macaque V1 to the pale cytochrome oxidase stripes of V2. J. Neurosci. *33*, 11530-11539.

Friston, K. (2005). A theory of cortical responses. Phil. Trans. R. Soc. Lond B Biol. Sci. *360*, 815-836.

Friston, K. (2008). Hierarchical models in the brain. PLoS Comput. Biol. *4*, e1000211.

Friston, K., and Kiebel, S. (2009). Predictive coding under the free-energy principle. Philos. Trans. R .Soc. Lond. B Biol. Sci. *364*, 1211-1221.

Glickfeld, L.L., Andermann, M.L., Bonin, V., and Reid, R.C. (2013). Cortico-cortical projections in mouse visual cortex are functionally target specific. Nat. Neurosci. *16*, 219-226.

Hawkins, J. (2004). On intelligence (New York, NY: Times Books).

Hubel, D.H., and Wiesel, T.N. (1962). Receptive fields, binocular interaction and functional architecture in the cat's visual cortex. J. Physiol. (Lond.) *160*, 106-154.

Huh, C.Y.L., Peach, J.P., Bennett, C., Vega, R.M., and Hestrin, S. (2018). Feature-Specific Organization of Feedback Pathways in Mouse Visual Cortex. Curr. Biol. *28*, 114-120 e115.

Hupé, J.M., James, A.C., Payne, B.R., Lomber, S.G., Girard, P., and Bullier, J. (1998). Cortical feedback improves discrimination between figure and background by V1, V2 and V3 neurons. Nature *394*, 784-787.

Landisman, C.E., and Ts'o, D.Y. (2002). Color processing in macaque striate cortex: relationships to ocular dominance, cytochrome oxidase, and orientation. J. Neurophysiol. *87*, 3126-3137.

Livingstone, M.S., and Hubel, D.H. (1984). Anatomy and physiology of a color system in the primate visual cortex. J. Neurosci. *4*, 309-356.

Livingstone, M.S., and Hubel, D.H. (1987). Connections between layer 4B of area 17 and the thick cytochrome oxidase stripes of area 18 in the squirrel monkey. J. Neurosci. *7*, 3371-3377.

Livingstone, M.S., and Hubel, D.H. (1988). Segregation of form, color, movement, and depth: anatomy, physiology, and perception. Science *240*, 740-749.

Lu, H.D., Chen, G., Tanigawa, H., and Roe, A.W. (2010). A motion direction map in macaque V2. Neuron *68*, 1002-1013.

Lu, H.D., and Roe, A.W. (2008). Functional organization of color domains in V1 and V2 of macaque monkey revealed by optical imaging. Cereb. Cortex *18*, 516-533.

Luck, S.J., Chelazzi, L., Hillyard, S.A., and Desimone, R. (1997). Neural mechanims of spatial selective attention in areas V1, V2 and V4 of macaque visual cortex. J. Neurophysiol. *77*, 24-42.

Luo, L., Callaway, E.M., and Svoboda, K. (2008). Genetic dissection of neural circuits. Neuron *57*, 634-660.

Maunsell, J.H., and Treue, S. (2006). Feature-based attention in visual cortex. Trends Neurosci. *29*, 317-322.

Maunsell, J.H.R., and Van Essen, D.C. (1983). The connections of the middle temporal visual area (MT) and their relationship to a cortical hierarchy in the macaque monkey. J. Neurosci. *3*, 2563-2586.

McAdams, C.J., and Reid, C.R. (2005). Attention modulates the responses of simple cells in monkey primary visual cortex. J. Neurosci. *25*, 11023-11033.

Moore, T., and Zirnsak, M. (2017). Neural Mechanisms of Selective Visual Attention. Annu. Rev. Psychol. *68*, 47-72.

Mumford, D. (1992). On the computational architecture of the neocortex. II. The role of cortico-cortical loops. Biol. Cybern. *66*, 241-251.

Nassi, J.J., Lomber, S.G., and Born, R.T. (2013). Corticocortical feedback contributes to surround suppression in V1 of the alert primate. J. Neurosci. *33*, 8504-8517.

Nurminen, L., Merlin, S., Bijanzadeh, M., Federer, F., and Angelucci, A. (2018). Top-down feedback controls spatial summation and response amplitude in primate visual cortex. Nature Commun *9*, 2281.

Rao, R.P., and Ballard, D.H. (1999). Predictive coding in the visual cortex: a functional interpretation of some extra-classical receptive-field effects. Nat. Neurosci. *2*, 79-87.

Rockland, K.S., and Knutson, T. (2000). Feedback connections from area MT of the squirrel monkey to areas V1 and V2. J. Comp. Neurol. *425*, 345-368.

Rockland, K.S., and Pandya, D.N. (1979). Laminar origins and terminations of cortical connections of the occipital lobe in the Rhesus monkey. Brain Res. *179*, 3-20.

Rockland, K.S., and Virga, A. (1989). Terminal arbors of individual "feedback" axons projecting from area V2 to V1 in the macaque monkey: a study using immunohistochemistry of anterogradely transported phaseolus vulgaris-leucoagglutinin. J. Comp. Neurol. *285*, 54-72.

Roe, A.W., Lu, H.D., and Chen, G. (2008). Functional architecture of area V2. In Encyclopedia of Neuroscience, L. Squire, ed. (Oxford, UK, Elsevier).

Roelfsema, P.R. (2006). Cortical algorithms for perceptual grouping. Ann. Rev. Neurosci. *29*, 203-227.

Shipp, S. (2016). Neural Elements for Predictive Coding. Front. Psychol. *7*, 1792.

Shmuel, A., Korman, M., Sterkin, A., Harel, M., Ullman, S., Malach, R., and Grinvald, A. (2005). Retinotopic axis specificity and selective clustering of feedback projections from V2 to V1 in the owl monkey. J. Neurosci. *25*, 2117-2131.

Sincich, L.C., and Horton, J.C. (2002). Divided by cytochrome oxidase: a map of the projections from V1 to V2 in macaques. Science *295*, 1734-1737.

Sincich, L.C., and Horton, J.C. (2005). The circuitry of V1 and V2: integration of color, form and motion. Ann. Rev. Neurosci. *28*, 303-326.

Sincich, L.C., Jocson, C.M., and Horton, J.C. (2007). Neurons in V1 patch columns project to V2 thin stripes. Cereb. Cortex *17*, 935-941.

Sincich, L.C., Jocson, C.M., and Horton, J.C. (2010). V1 interpatch projections to V2 thick stripes and pale stripes. J. Neurosci. *30*, 6963-6974.

Siu, C., Merlin, S., Federer, F., and Angelucci, A. (2018). A direct feedback-to-feedforward circuit for fast feedback modulation of incoming feedforward signals. SFN Abstracts online *219.22*.

Stettler, D.D., Das, A., Bennett, J., and Gilbert, C.D. (2002). Lateral connectivity and contextual interactions in macaque primary visual cortex. Neuron *36*, 739-750.

Tootell, R.B., Nelissen, K., Vanduffel, W., and Orban, G.A. (2004). Search for color "center(s)" in macaque visual cortex. Cereb. Cortex *14*, 353-363.

Tootell, R.B., Silverman, M.S., Hamilton, S.L., De Valois, R.L., and Switkes, E. (1988). Functional anatomy of macaque striate cortex. III. Color. J. Neurosci. *8*, 1569-1593.

Ts'o, D.Y., and Gilbert, C.D. (1988). The organization of chromatic and spatial interactions in the primate striate cortex. J. Neurosci. *8*, 1712-1727.

Van Essen, D.C., and Maunsell, J.H.R. (1983). Hierarchical organization and functional streams in the visual cortex. Trends Neurosci. *6*, 370-375.

Wang, Y.I., Xiao, Y., and Felleman, D.J. (2007). V2 thin stripes contain spatially organized representations of achromatic luminance change. Cereb. Cortex *17*, 116-129.

Xiao, Y., Casti, A., Xiao, J., and Kaplan, E. (2007). Hue maps in primate striate cortex. Neuroimage *35*, 771-786.

Xiao, Y., Wang, Y.I., and Felleman, D.J. (2003). A spatially organized representation of color in macaque cortical area V2. Nature *421*, 535-439.

Yoshioka, T., and Dow, B.M. (1996). Color, orientation and cytochrome oxidase reactivity in areas V1, V2 and V4 of macaque monkey visual cortex. Behav. Brain Res. *76*, 71-88.

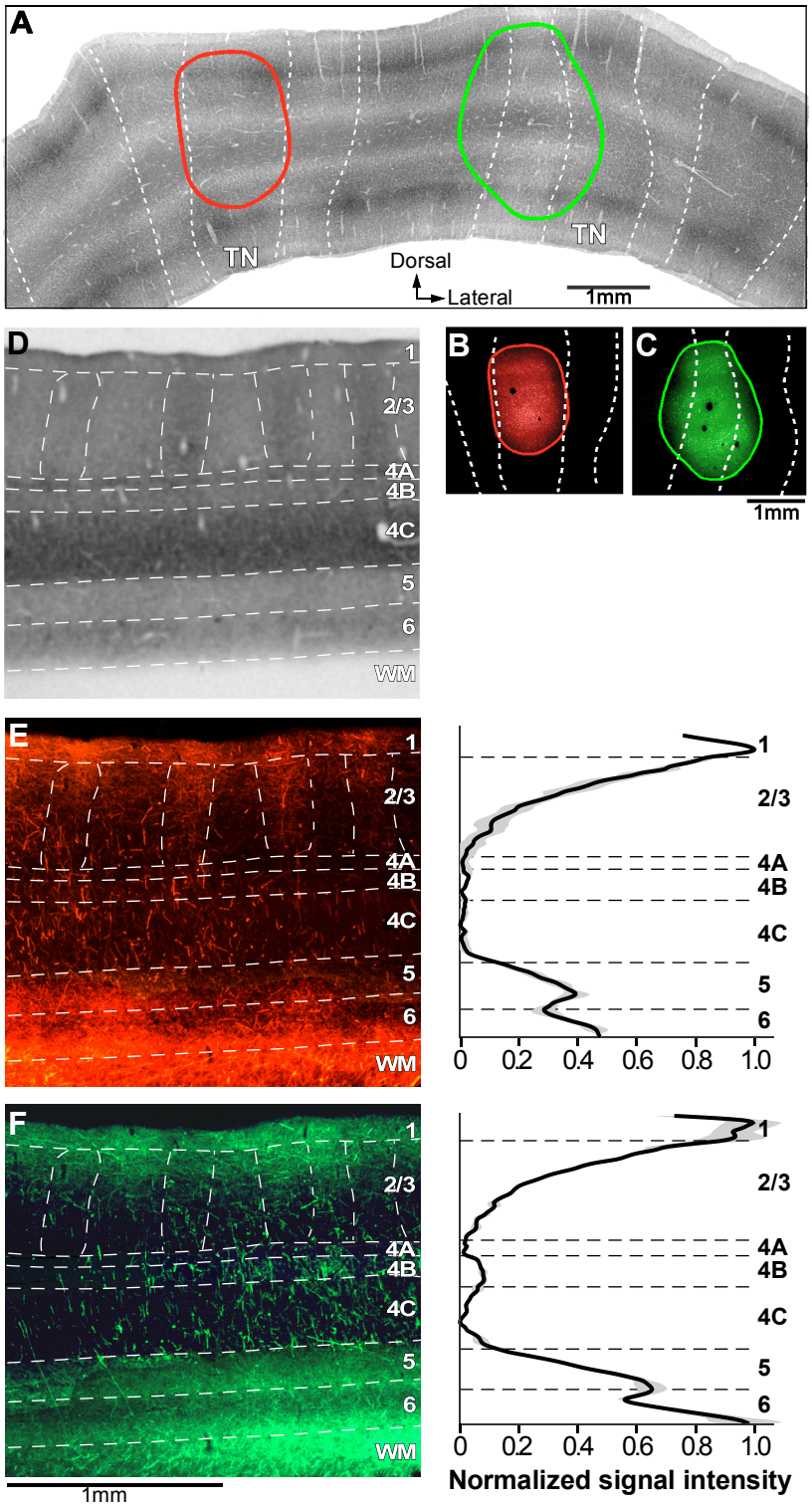
A
TN
TN
Dorsal
Lateral
1mm
D
1
2/3
4A
4B
4C
5
6
WM
B
C
1mm
E
F
1mm
0
0.2
0.4
0.6
0.8
1.0
Normalized signal intensity

Figure 1

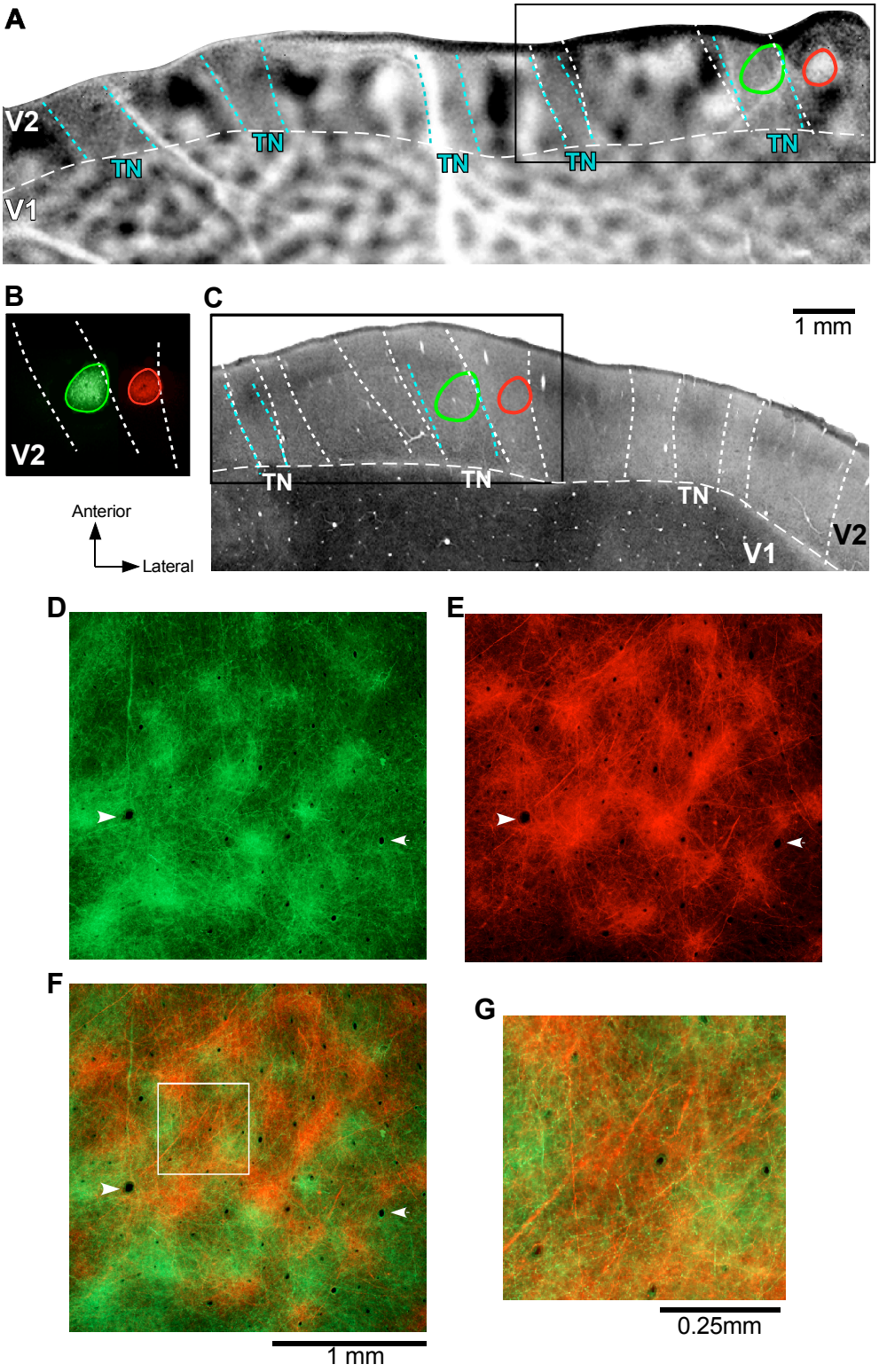
A
V2
V1
TN
TN
TN
TN
TN
B
V2
C
1 mm
TN
TN
TN
V1
V2
Anterior
Lateral
D
E
F
1 mm
G
0.25mm

Figure 2

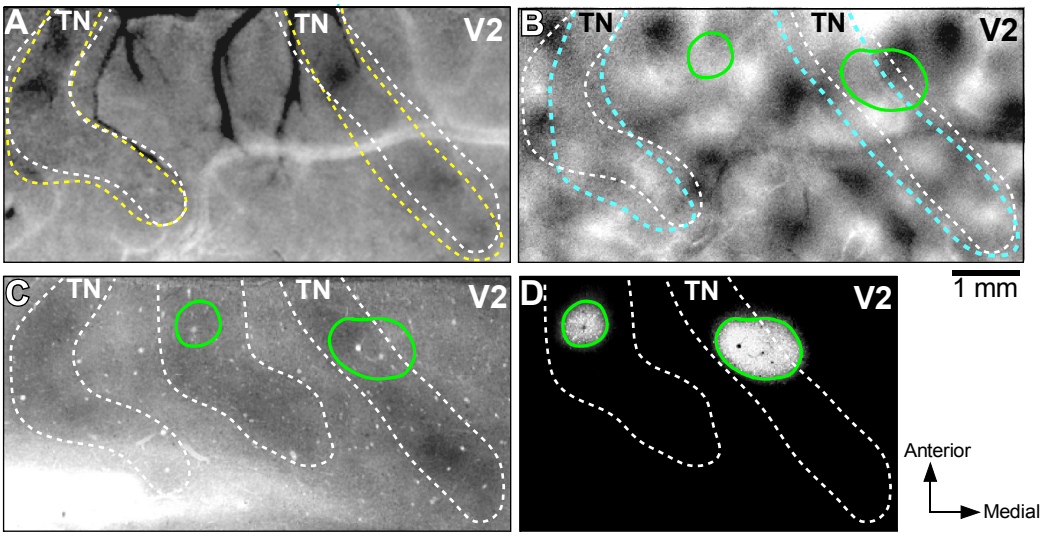

Figure 3

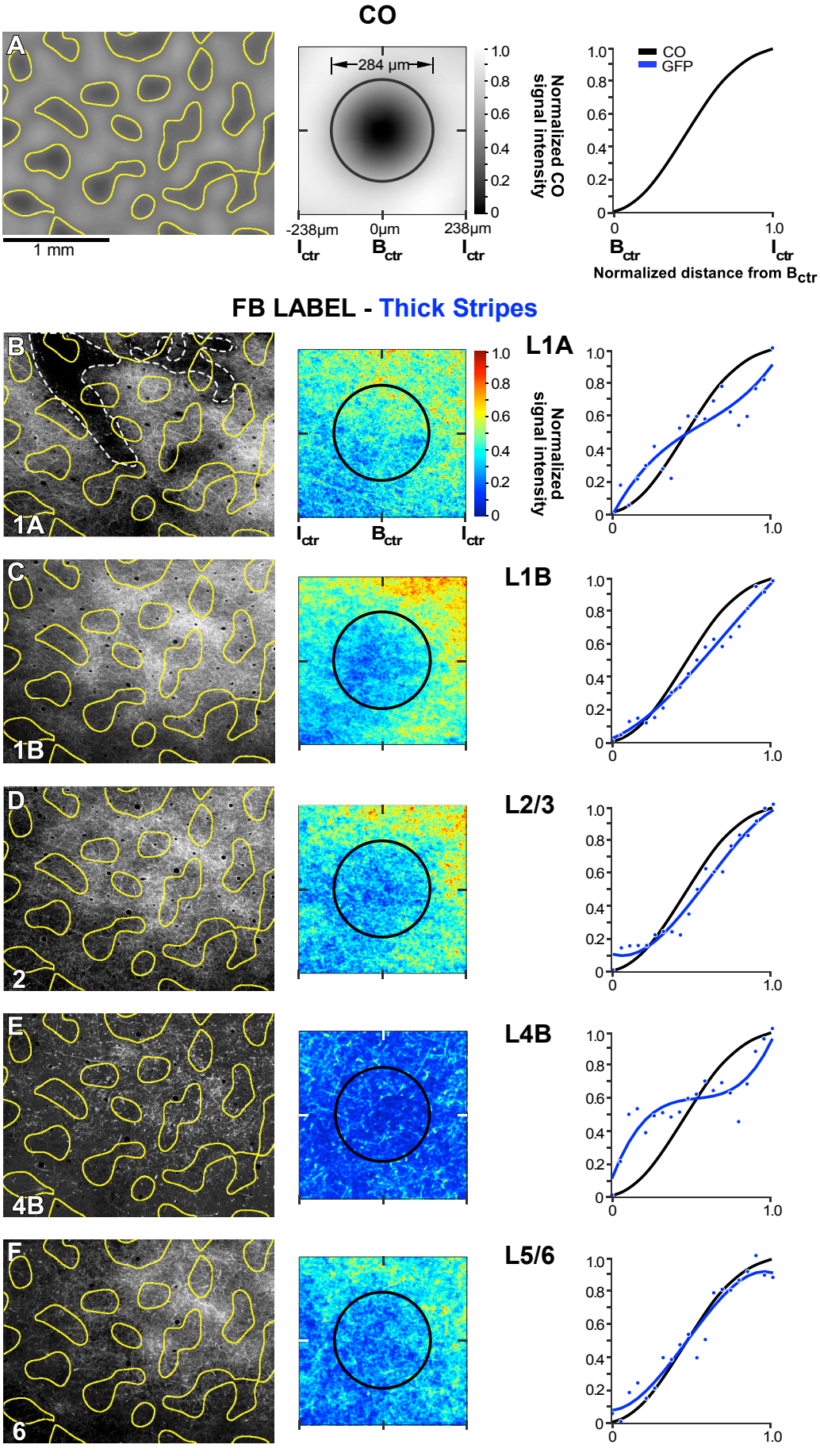
CO
A
1 mm
284 µm
-238µm
0µm
238µm
I_{ctr}
B_{ctr}
I_{ctr}
Normalized CO signal intensity
CO
GFP
Normalized distance from B_{ctr}
FB LABEL - Thick Stripes
B
1A
L1A
Normalized signal intensity
C
1B
L1B
D
2
L2/3
E
4B
L4B
F
6
L5/6

Figure 4

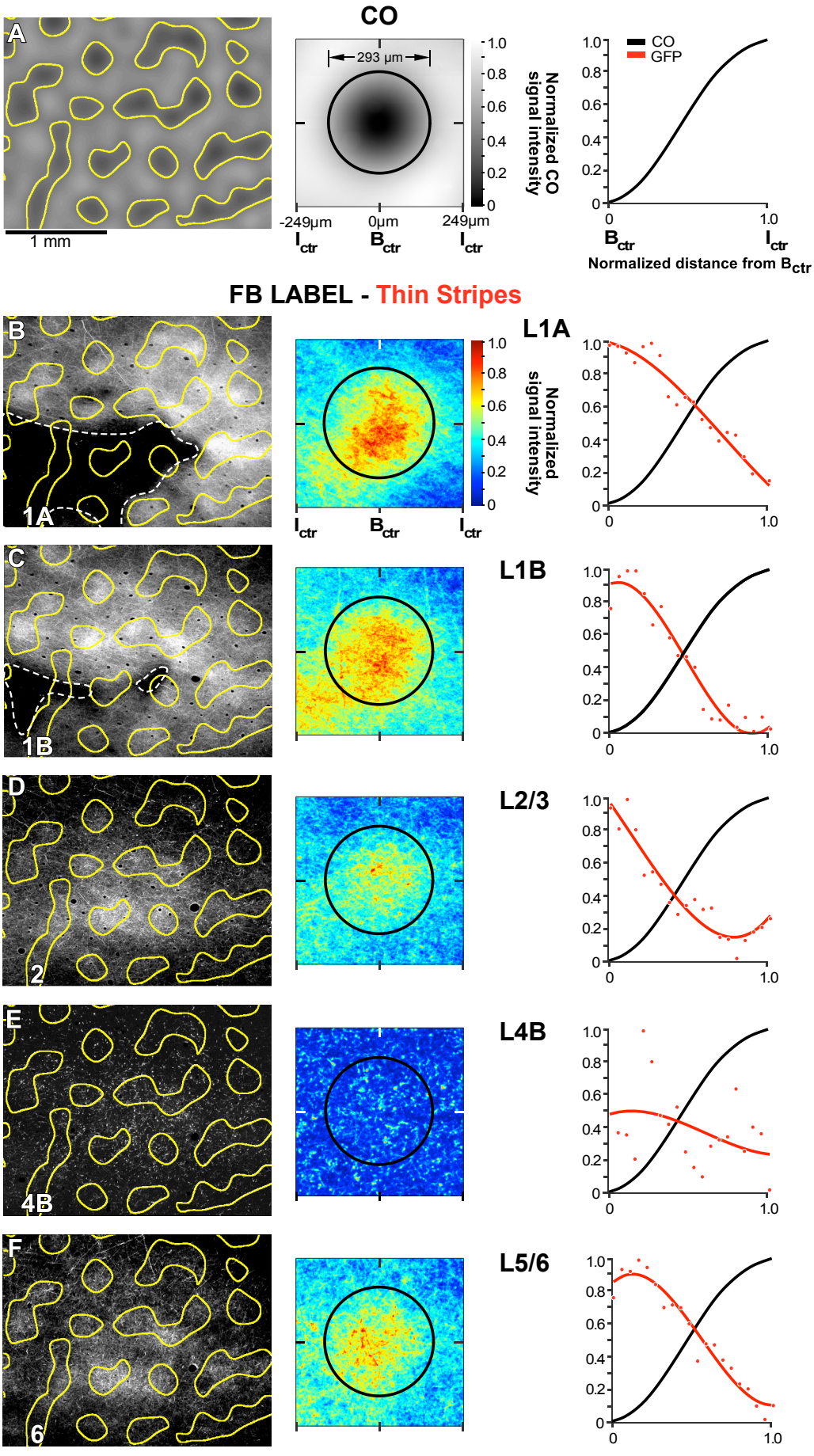
A
1 mm
CO
293 µm
-249µm
0µm
249µm
I_{ctr}
B_{ctr}
I_{ctr}
Normalized CO signal intensity
CO
GFP
B_{ctr}
I_{ctr}
Normalized distance from B_{ctr}
FB LABEL - Thin Stripes
B
1A
L1A
Normalized signal intensity
C
1B
L1B
D
2
L2/3
E
4B
L4B
F
6
L5/6

Figure 5

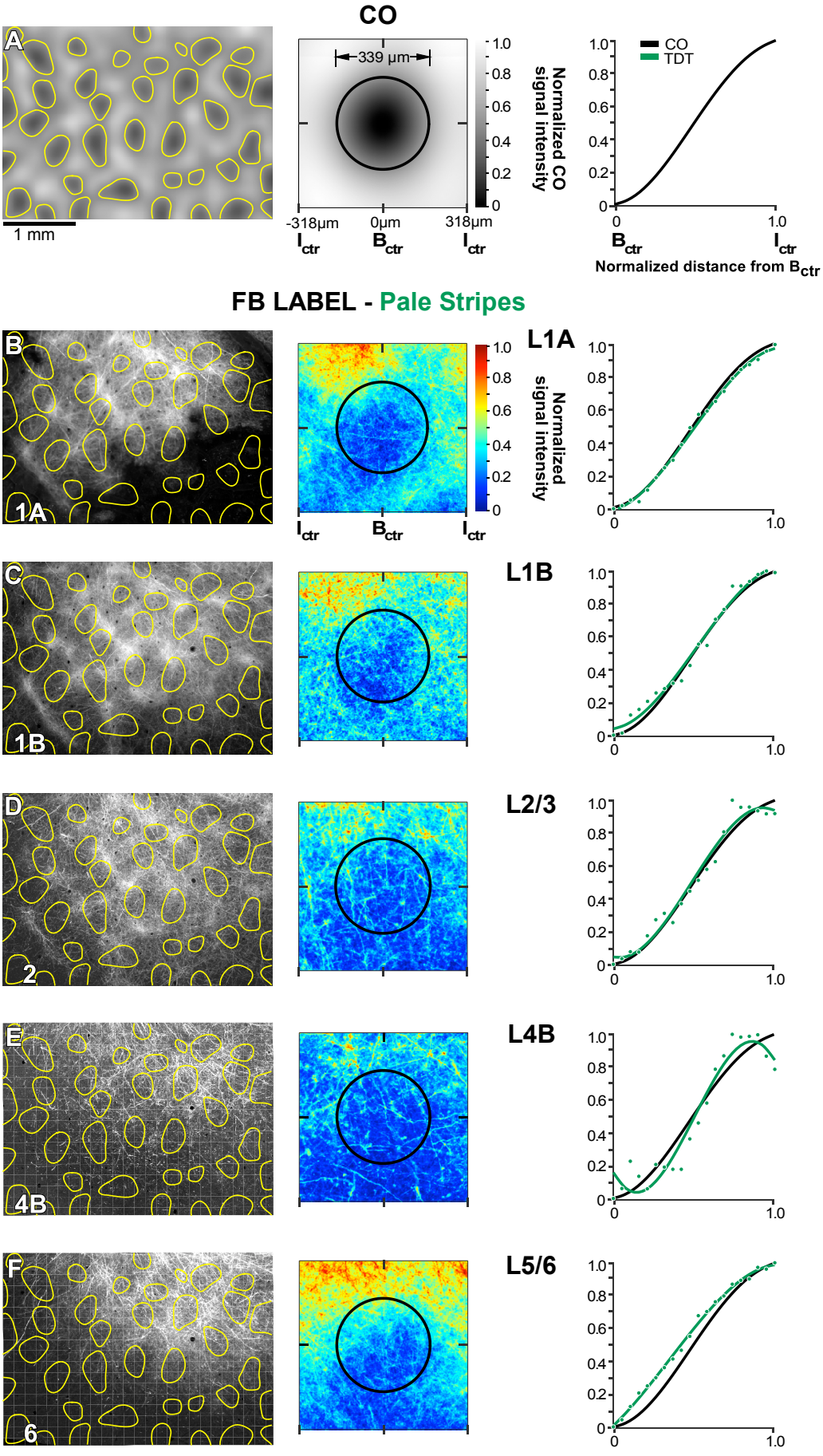
CO
A
1 mm
339 µm
-318µm
0µm
318µm
I_{ctr}
B_{ctr}
I_{ctr}
Normalized CO signal intensity
CO
TDT
B_{ctr}
I_{ctr}
Normalized distance from B_{ctr}
FB LABEL - Pale Stripes
B
1A
L1A
Normalized signal intensity
C
1B
L1B
D
2
L2/3
E
4B
L4B
F
6
L5/6

Figure 6

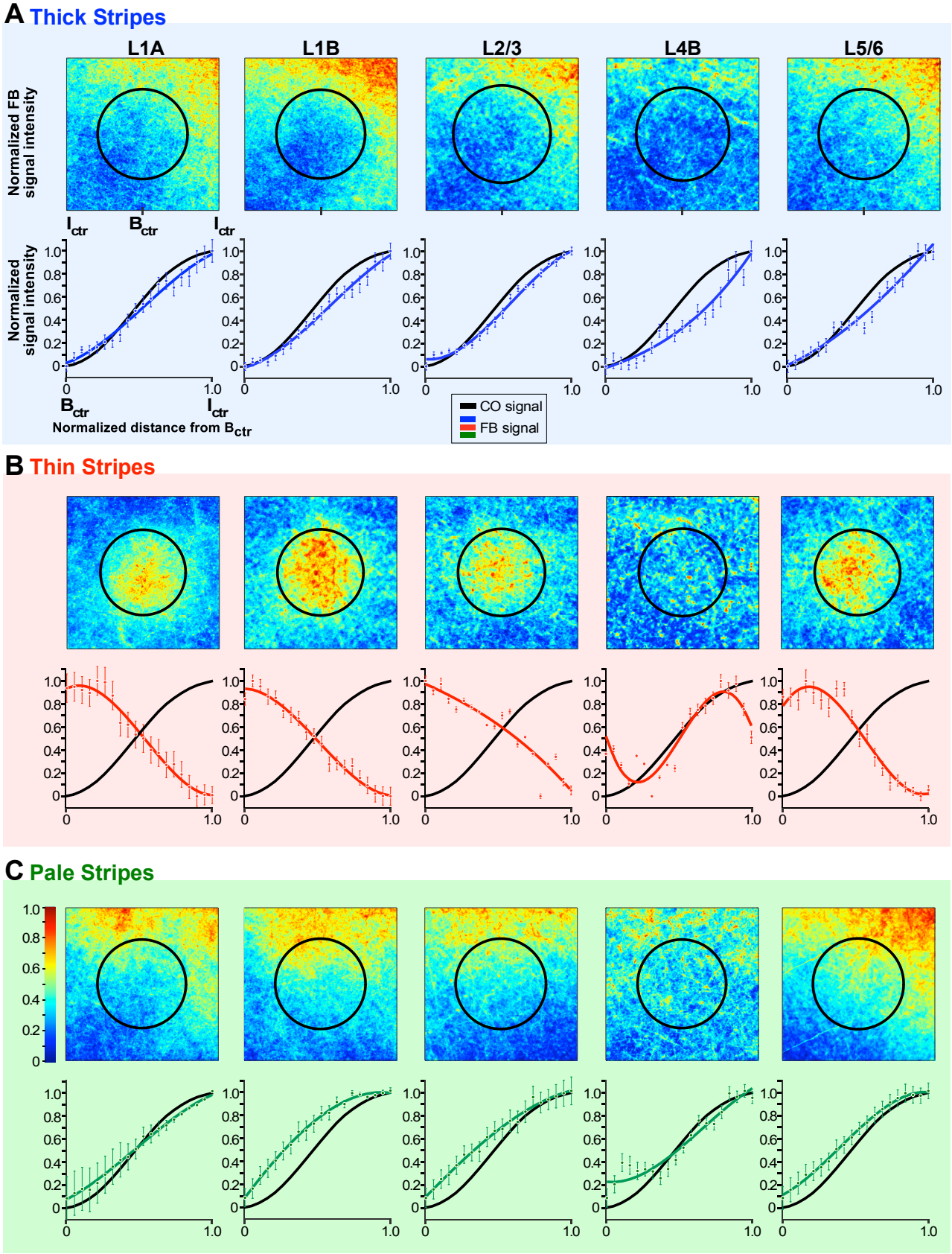
A Thick Stripes
L1A
L1B
L2/3
L4B
L5/6
Normalized FB signal intensity
Normalized signal intensity
Normalized distance from Bctr
CO signal
FB signal
B Thin Stripes
C Pale Stripes

Figure 7

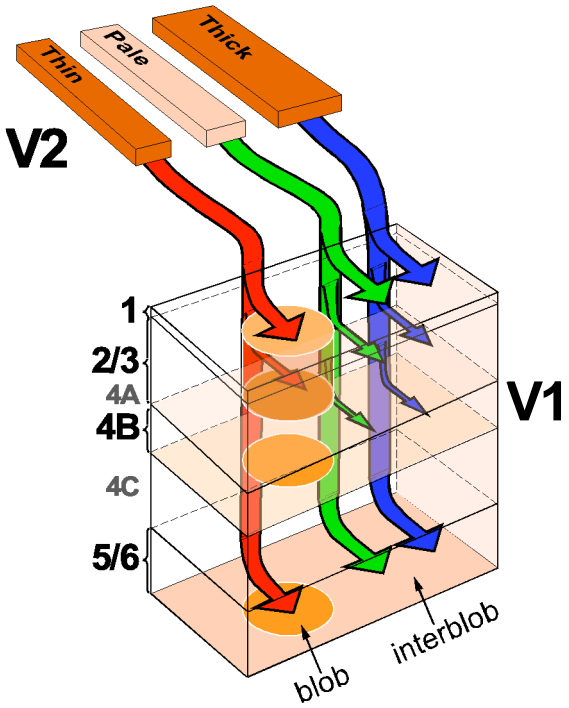

Figure 8

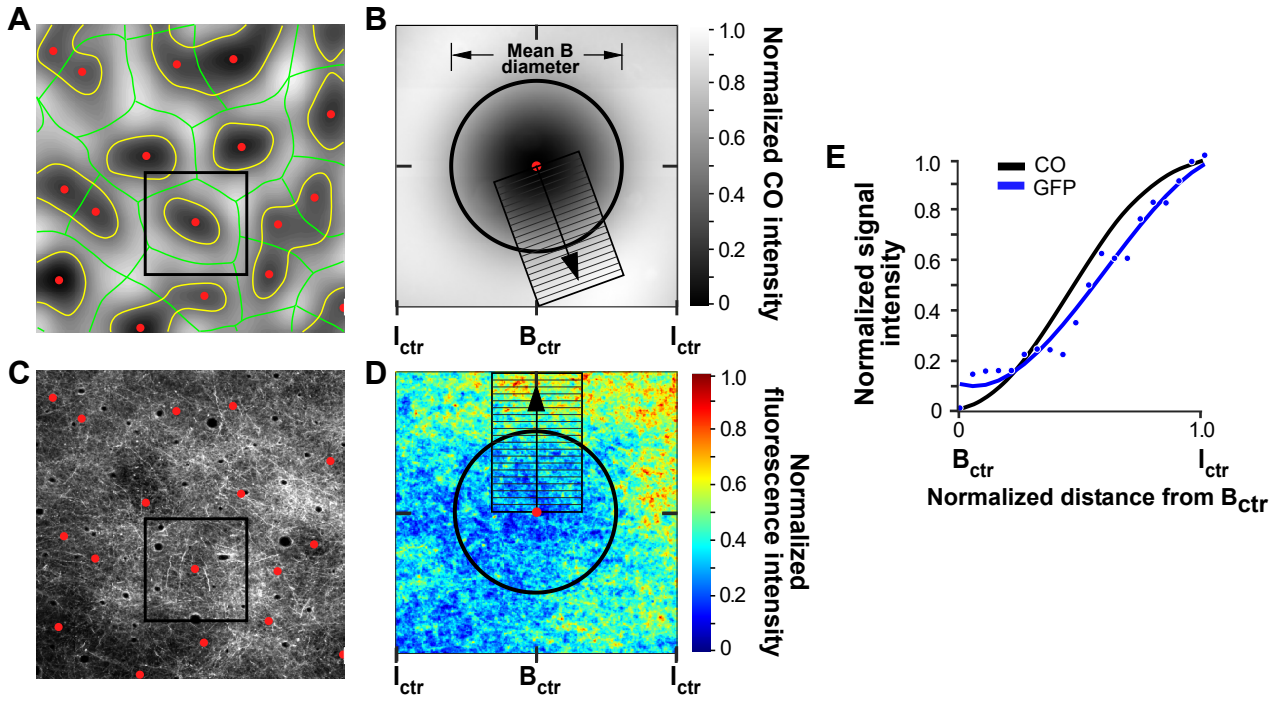

Figure S1 (Related to Figs. 4-6)

Quantitative analysis of the distribution of FB axons across V1 CO compartments.
(A) Filtered CO stained section through L2/3 of V1. *Yellow and green contours and red dots* mark the blob borders, interblob and blob centers, respectively, extracted as described in the Star Methods. All blobs and interblobs in this map overlap the region containing labeled FB axons shown in (C) and were used to compute the heat map shown in (D). B*lack box:* an ROI, representing the average size of a blob and interblob in the larger CO map encompassing the full extent of the labeled FB fields across all layers. This ROI was centered on each blob in (A) and used to compute fluorescent signal intensity in (D). **(B)** Heat map of CO intensity, obtained by summing CO intensity across all blob ROIs for the case, and normalizing to maximum intensity. *Black circle*: mean blob diameter for all blobs used to compute the heat map. *Black box:* a 200 µm-wide window, centered on the region of highest CO intensity in the heat map, was divided into 20 bins from the blob center to the interblob center in the heat map. The mean signal intensity in each bin was normalized to the highest intensity value across all bins and plotted as a function of distance from the blob center (B_{ctr}) in panel E (*black curve*). **(C)** Digitized image of GFP-labeled FB axons in a section through L2/3 of V1, vertically aligned to the CO section shown in (A). *Red dots* mark the blob centers from (A). The fluorescent signal intensity was measured in this section within the ROI from (A) centered on each blob overlaying the FB label in the layer. **(D)** Heat map of fluorescent signal intensity obtained by summing fluorescent intensity across all blob ROIs in (C), and normalizing to maximum intensity. *Black circle:* average blob diameter computed from all blobs in (A). The *black box* is the region of highest fluorescence intensity in the heat map, and was used to generate the plot of fluorescence intensity as a function of distance from the B_{ctr} in panel E (*blue curve*). **(E)** Plots of normalized CO and fluorescent signal intensities as a function of distance from the B_{ctr}, measured within the black boxes shown in (B) and (D), respectively.